Article

High Pressure−Temperature Study of MgF$_2$, CaF$_2$, and BaF$_2$ by Raman Spectroscopy: Phase Transitions and Vibrational Properties of AF$_2$ Difluorides

Xinyue Zhang, Luo Li, Yingxin Yu, Qingchun Zhang, Ningyu Sun,* Zhu Mao, and Dongzhou Zhang

Read Online

ACCESS | Metrics & More | Article Recommendations | SI Supporting Information

ABSTRACT: The phase transition of AF$_2$ difluorides strongly depends on pressure, temperature, and cationic radius. Here, we have investigated the phase transition of three difluorides, including MgF$_2$, CaF$_2$, and BaF$_2$, at simultaneously high pressures and temperatures using Raman spectroscopy and X-ray diffraction in externally heated diamond anvil cells up to 55 GPa at 300−700 K. Rutile-type difluoride MgF$_2$ with a small cationic radius undergoes a transition to the CaCl$_2$-type phase at 9.9(1) GPa and 300 K, to the HP-PdF$_2$-type phase at 21.0(2) GPa, and to the cotunnite-type phase at 44.2(2) GPa. The phase transition pressure to the HP-PdF$_2$ and cotunnite structure at 300 K for our single crystal was found to be higher than that in previous studies using polycrystalline samples. Elevating the temperature increases the transition pressure from rutile- to the CaCl$_2$-type phase but has a negative influence on the transition pressure when MgF$_2$ transforms from the HP-PdF$_2$- to cotunnite-type phase. Meanwhile, the transition pressure from the CaCl$_2$- to HP-PdF$_2$-type phase for MgF$_2$ was identified to be independent of the

temperature. Raman peaks suspected to belong to the α-PbO$_2$-type phase were observed at 14.6−21.0(1) GPa and 400−700 K. At 300 K, difluorides CaF$_2$ and BaF$_2$ in the fluorite structure with larger cationic radii transform to the cotunnite-type phase at 9.6(3) and 3.0(3) GPa at 300 K, respectively, and BaF$_2$ further undergoes a transition to the Ni$_2$In-type phase at 15.5(4) GPa. For both CaF$_2$ and BaF$_2$, elevating the temperature leads to a lower transition pressure from fluorite- to the cotunnite-type phase but has little influence on the transition to the Ni$_2$In structure. Raman data provide valuable insights for mode Grüneisen parameters. We note that the mode Grüneisen parameters for both difluorides and dioxides vary linearly with the cation radius. Further calculations for the mode Grüneisen parameters at high pressures for MgF$_2$, CaF$_2$, and BaF$_2$ yield a deeper understanding of the thermodynamic properties of the difluorides.
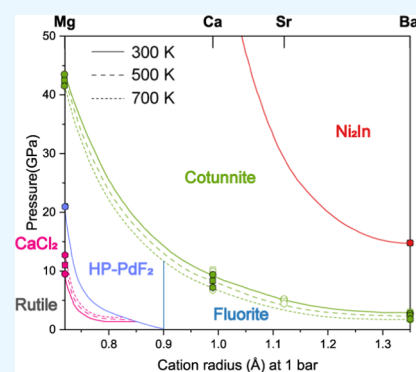
1. INTRODUCTION

AF$_2$ difluorides, in which cation A represents group-II alkaline earth (i.e., Mg, Ca, Sr, and Ba) and transition metal elements (i.e., Zn, Co, and Mn), are widely used as optical components and luminescent materials owing to their desirable optical and mechanical properties.[1,2] The structure of the difluorides exhibits systematic dependence on ionic radii of cations and electronic properties.[3−5] Influenced by the geometry and the mutual contact of the large anions, difluorides with larger ionic radii of cations tend to have higher coordination at ambient conditions.[5,6] When the cation radius ranges from 0.9 to 1.35 Å, difluorides normally crystallize in the cubic fluorite-type structure ($Fm\overline{3}m$, $Z = 4$) with a coordination number of 8.[5,7−9] As the cationic radius drops below 0.9 Å, the inability of contact between the anion and cation reduces the repulsive forces balancing the Coulomb forces in this high-coordination structure, resulting in a tetragonal rutile-type structure ($P4_2/mnm$, $Z = 2$) for these difluorides.[3−6,10−12] Of particular interest is the same rutile-type structure of some dioxides, such as SiO$_2$, TiO$_2$, etc., as difluorides at ambient conditions.[13−15] These oxides are important rock-forming minerals in the

earth's deep interior, following a similar high-pressure transition sequence of rutile-type difluorides but much higher transition pressure.[16−18] Difluorides are thus regarded as good analogues of dioxides in earth sciences.[19,20] Therefore, the complex polymorphism and unique physical properties of difluorides under extreme conditions have captivated wide attention.[21]

The phase transition sequence of difluorides at high pressures is strongly dependent on the cation radius.[3−5,7,10,12,22] At 300 K, rutile-type difluorides such as MgF$_2$ with a small cation radius of 0.72 Å undergo a second-order transformation to the orthorhombic CaCl$_2$-type structure ($Pnnm$, $Z = 2$) at ∼9 GPa and then transforms to the cubic HP-PdF$_2$-type structure ($Pa\overline{3}$, $Z = 4$, also misidentified as a

"pyrite-type" structure in some studies) at ~14 GPa.[10,23,24] However, an additional α-PbO$_2$-type phase was predicted by theoretical calculation to be stable between CaCl$_2$- and HP-PdF$_2$-type phases.[10] Further elevating pressure to ~38 GPa leads to the transition to the cotunnite-type structure (*Pnma*, *Z* = 4).[10,25−27] Increasing the cation radius leads to a decrease in the phase transition pressure to CaCl$_2$- and HP-PdF$_2$-type structures.[3,4] For example, ZnF$_2$ with a cation radius of 0.74 Å transitions to the CaCl$_2$-type phase at 4.5 GPa and to the HP-PdF$_2$-type structure at 10 GPa, which are much lower than those of MgF$_2$ at 300 K.[4,28] Of particular interest is the rutile-type MnF$_2$, which transforms to the ZrO$_2$- or SrI$_2$-type rather than CaCl$_2$-type structure at ~3 GPa.[12,29] In contrast to the HP-PdF$_2$-type MgF$_2$, which directly transitions into the cotunnite structure at higher pressures, some transition metal difluorides like ZnF$_2$ and CoF$_2$ will transform into the AgF$_2$- or cubic fluorite-type structures before changing to the cotunnite structure.[3,4]

When the cation radius is greater than 0.9 Å, the fluorite-type difluorides will transition into the cotunnite-type structure at high pressures.[5,30−34] CaF$_2$ with a relatively small cation radius of 0.99 Å has a transition pressure of 9 GPa at 300 K, while SrF$_2$ with a large cation radius of 1.12 Å has a lower transition pressure of 5 GPa.[5] BaF$_2$ has the largest cation radius of 1.35 Å among this group, and the transition pressure is the lowest (3 GPa).[5,35,36] Difluorides in cotunnite-type structure will further transition into the hexagonal Ni$_2$In-type phase (*P6$_3$/mmc*, *Z* = 2) at higher pressures.[5,34,36] The transition pressure of CaF$_2$ is 72 GPa, which is much greater than those of SrF$_2$ (29 GPa) and BaF$_2$ (14 GPa).[5] For PbF$_2$, the cotunnite-type phase will transform to a 10-fold Co$_2$Si structure at 22 GPa rather than a Ni$_2$In-type structure.[22]

Temperature also plays a key role in the structure of difluorides.[30,37,38] At 1 bar, rutile-type difluorides like MgF$_2$ tend to retain their original phase at high temperatures up to 1100 K.[37] In contrast, fluorite-type difluorides such as CaF$_2$, SrF$_2$, and BaF$_2$ undergo a phase transition from the fluorite phase to the superionic state at 1100−1400 K and ambient pressures.[30−33,38−41] For rutile-type difluorides, the experiments at simultaneously high pressure−temperature (*P−T*) conditions were only conducted on MgF$_2$, ZnF$_2$, and MnF$_2$ using the X-ray diffraction (XRD) method to investigate their structure stability up to 15 GPa and 750 °C.[29,42,43] Of particular interest is the different structures observed in these difluorides at high *P−T* conditions.[29,42,43] The XRD measurement in the large-volume apparatus has been conducted in MgF$_2$ up to 15 GPa and 750 °C, which indicated that the α-PbO$_2$-type phase of MgF$_2$ was partially transformed from the CaCl$_2$-type phase at 13 GPa and 600 °C and became a single phase at 12.7 GPa and 750 °C.[43] However, there are only one or two scattered experimental points for each phase of MgF$_2$, making it difficult to determine the Clapeyron slopes of the phase boundaries.[43] The study about MnF$_2$ focuses on the high-pressure behavior upon decompression at high temperatures.[29] Interestingly, it has been observed that the α-PbO$_2$-type phase and a phase with the space group $P\overline{4}_2m$ are stable between 1 and 4 GPa at 500−700 K during the decompression process.[29]

For fluorite-type difluorides, the experiments at high *P−T* conditions have been conducted on CaF$_2$, SrF$_2$, and BaF$_2$ using differential thermal analysis or by measuring dielectric properties up to 6.0 GPa and 2200 K.[39−41] These studies indicated that CaF$_2$, SrF$_2$, and BaF$_2$ exhibit the fluorite-to-

cotunnite phase transition at temperatures up to ~1300 K with a slightly negative Clapeyron slope, which also been supported by recent theoretical calculation.[30−33,38−41] The experiments were also conducted on PbF$_2$ by laser-heating XRD methods up to 64.5 GPa and 2430 K.[22] Different from the transition sequence at room temperature, cotunnite-type PbF$_2$ will transform to a Ni$_2$In-type structure at 25.9 GPa after heating to 1400 K.[22] However, the high *P−T* results related to higher pressure, which may show a distinct phase transition, are still scarce for most difluorides with alkaline earth elements. To better understand the impact of temperature on the phase boundary of AF$_2$ difluorides, it is crucial to experimentally investigate their high-pressure behavior under simultaneously high *P−T* conditions.

In this study, we investigated the phase transition of three difluorides, including MgF$_2$, CaF$_2$, and BaF$_2$, at simultaneously high *P−T* conditions using Raman spectroscopy and XRD up to 55 GPa and 700 K in diamond anvil cells (DACs). These representative difluorides have cationic radii in the range of 0.72−1.35 Å, which can systematically reveal the influence of the cationic radius at high *P−T* conditions on the structure of difluorides. Our experimental results provide crucial constraints on the phase boundary and mode Grüneisen parameters of these difluorides at high *P−T* conditions. Together with previous experimental results, we provide a more comprehensive understanding of the influence of pressure, temperature, and cation radius on the structure of difluorides.

2. EXPERIMENTAL DETAILS

Single-crystal MgF$_2$, CaF$_2$, and BaF$_2$ (purity 99.99%) were purchased from Hefei Kejing Materials Technology Co., Ltd. All of the sample crystals were double-sided polished to 20−30 μm in thickness for high *P−T* Raman measurements. For all three difluorides, a number of sample pieces with different crystal orientations, including some specific orientations, such as (100), (111), and (001), were prepared for the measurements. For MgF$_2$, we prepared additional platelets ~10 μm in thickness for XRD measurements.

High-pressure Raman and XRD measurements at 300 K were conducted using short symmetric diamond anvil cells (DACs) equipped with a pair of 300, 400, or 500 μm culet diamonds. The sample platelets were loaded into the center of the diamond culets, and rhenium was used as the gasket material. The gasket holes with radii of 165, 210, and 295 μm were laser-drilled for 300, 400, or 500 μm culet diamonds, respectively. For Raman measurements, one or two small ruby spheres were loaded into each sample chamber for pressure determination.[44] For XRD measurements, Au was used as the pressure calibrant.[45] Argon was used to provide a quasi-hydrostatic environment for all of the Raman and XRD measurements below 40 GPa, while neon was used for measurements greater than 40 GPa.[46,47] To explore the combined effect of *P−T* on the structure of difluorides, the samples were loaded into the BX90-type externally heated DACs (EHDACs) for high *P−T* measurements, while the size of the diamond culets, gasket, and the hydrostatic pressure transmitting media were same as the high-pressure and 300 K measurements.[48] Due to the increased line width of the fluorescence lines and reduced accuracy of ruby's signal above ~550 K, we used cubic boron nitride (cBN) as the pressure calibrant for high-temperature Raman measurements.[49] The pressure difference before and after the measurement was less
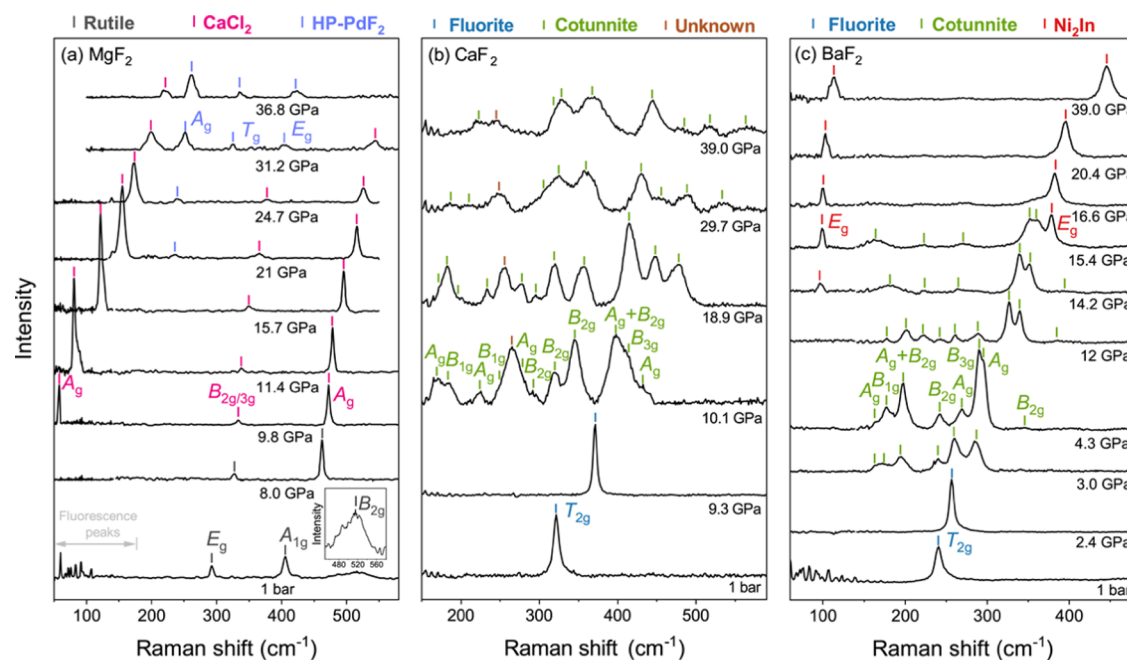
Figure 1. Raman spectra of difluorides at high pressures and 300 K. (a) MgF_2. The weak B_{2g} mode of the rutile-type structure at ambient conditions is enlarged as an illustration. (b) CaF_2. (c) BaF_2. The short lines with different colors indicate the position of different Raman modes.

Table 1. Raman Frequencies ν (cm^{-1}), First-Order and Second-Order Pressure Coefficients ($d\nu/dp$ (cm^{-1}/GPa) and $d^2\nu/dp^2$ (cm^{-2}/GPa^2), Respectively), and Mode Grüneisen Parameter γ of the Rutile- (1 bar), $CaCl_2$- (9.9 GPa), HP-PdF$_2$- (31.2 GPa), and α-PbO$_2$-Type Phase (1 bar) of MgF_2 at 300 K[a]

phase	mode symmetry	ν	ν_0 (fit)	$d\nu/dp$	$d^2\nu/dp^2$	γ_i
rutile (1 bar)	E_g	292.9(1)	294.3(6)	4.1(1)		1.42
	A_{1g}	405.6(1)	407.7(7)	6.8(1)		1.68
	B_{2g}	511.2(6)				
$CaCl_2$ (9.9 GPa)	A_g	58(1)	−41(4)	12.3(4)	−0.15(1)	20.10
	B_{2g}	333.2(3)	307.2(1)	2.79(5)		1.17
	B_{3g}	333.2(3)	307.2(1)	2.79(5)		1.17
	A_g	472.3(1)	421(1)	5.7(1)	−0.058(3)	1.34
HP-PdF$_2$ (31.2 GPa)	A_g	251.1(2)	198.0(8)	1.74(2)		1.64
	T_g	325.4(5)	240(14)	2.8(4)		2.02
	E_g	404.2(9)	290(3)	3.6(1)		1.77
α-PbO$_2$ (1 bar)		186.4(3)	186.7(7)	0.2(1)		
		254.4(8)	256.0(7)	1.0(1)		

[a]The fitting values of zero-pressure frequency are also displayed for different modes.

than 0.5 GPa. A K- or R-type thermocouple was attached to the surface of the diamond 500 μm from the diamond culet to determine the temperature (Figure S1). The uncertainty of the temperature in the EHDAC was within ±5 K.

Raman signals were excited by a 532 nm wavelength laser of 200 mW output power, and Raman measurements were conducted at the High-Pressure Mineral Physics Laboratory, University of Science and Technology of China (USTC). The phonon wavelengths were calibrated using the Raman spectrum of the peak of silica at 520.5 cm^{-1}, and the uncertainty was within ±0.5 cm^{-1}. At ambient conditions, all of the Raman spectra were collected without using the DACs. For MgF_2, the acquisition time for each Raman spectrum was 30 s, and we normally collected five spectra at given $P-T$ conditions. For CaF_2 and BaF_2, the acquisition time is ∼10 s with 5 to 10 accumulations. At high pressures, Raman measurements were performed at an interval of ∼1 to ∼40 GPa. After the compression experiments, all of the samples were decompressed to 1 bar, and the spectra were collected every 5 GPa during decompression. For simultaneously high $P-T$ experiments, Raman spectra were collected between 300 and 700 K in 50 K steps at a given pressure. The temperature increase rate was 0.3 K/s. After reaching the target temperature, the temperature was held for 3−10 min before starting measurements. After the compression experiments, the temperature was quenched to 300 K, and samples were decompressed to 1 bar.

We performed additional XRD measurements for single-crystal MgF_2 up to 55 GPa and 700 K at the 13-BM-C beamline of the GSECARS, Advanced Photon Source (APS), Argonne National Laboratory (wavelength: 0.4340 Å), and BL15U1 of Shanghai Synchrotron Radiation Facility (SSRF; wavelength: 0.6199 Å). At both facilities, diffraction images were collected using a MAR165 CCD detector.[50,51] At the 13-BM-C beamline of the GSECARS, the distance between the sample and the CCD detector was 196.4974 mm, and LaB$_6$
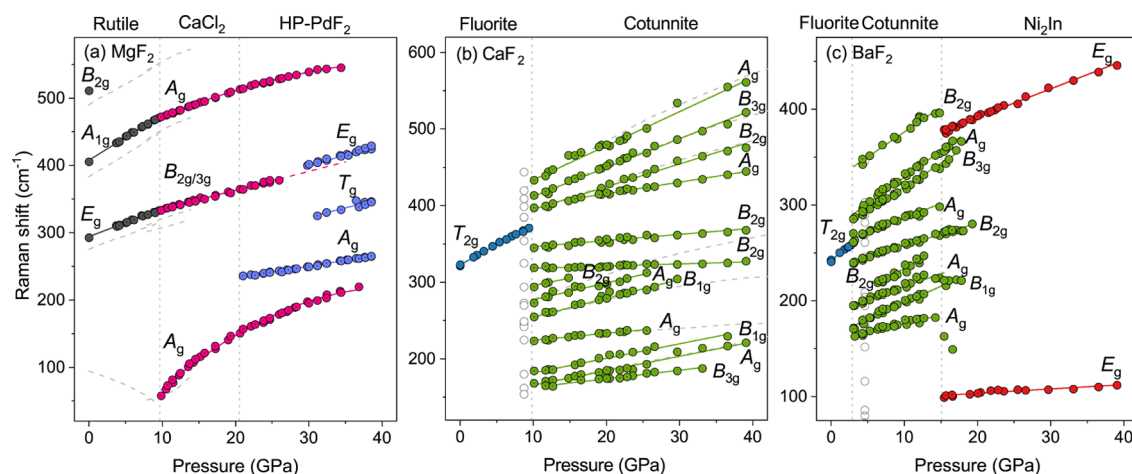
Figure 2. Raman shifts of high-pressure phases for difluorides at 300 K. (a) MgF$_2$. Black: rutile-type phase; pink: CaCl$_2$-type phase; purple: PdF$_2$-type phase; gray dashed lines: the calculated frequencies from Zhang et al.[52] (b) CaF$_2$. Blue: fluorite-type phase; green: cotunnite-type phase; gray open circles: the calculated frequencies from Chernyshev et al.;[53] gray dashed lines: the experimental results from Speziale and Duffy.[34] (c) BaF$_2$. Blue: fluorite-type phase; green: cotunnite-type phase; red: Ni$_2$In-type phase; gray open circles: the calculated frequencies from Chernyshev et al.[53] Solid circles: experimental data for samples with different orientations; solid lines: fitting results; gray dotted lines: the phase boundary of different phases.
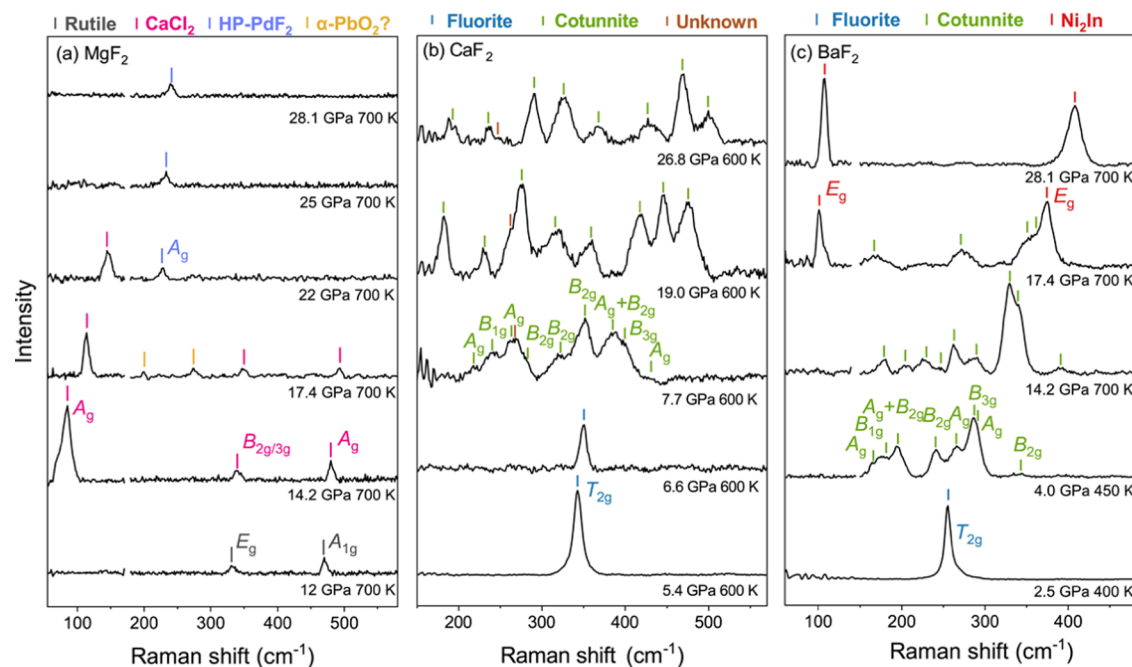

Figure 3. Raman spectra of difluorides at high $P-T$. (a) MgF$_2$. (b) CaF$_2$. (c) BaF$_2$. The short lines with different colors indicate the positions of different Raman modes.

powder was used as diffraction calibration, while at the BL15U1 of SSRF, the sample–detector distance was 133.2123 mm, which was calibrated using a CeO$_2$ standard. The XRD patterns at 300 K were collected up to 55 GPa with a pressure interval of 1–2 GPa. For high $P-T$ experiments, we first cold-compressed the sample to ∼4 GPa and then gradually increased the temperature. The XRD patterns were collected in a 100 K step from 300 to 700 K at each pressure. The temperature rising rate was the same as Raman measurements (0.3 K/s), while the temperature was only held for 0.5–3 min before data collection. The exposure time for the acquisition was 10–30 s, while the sample stage was rotated from −15 to 15° during data acquisition to obtain more diffraction spots.

3. RESULTS

3.1. MgF$_2$. Under ambient conditions, two distinct Raman peaks at 292.9(1) and 405.6(1) cm^{-1} were observed in all of the samples with different orientations for MgF$_2$, while an additional low-intensity wide band at 511.2(6) cm^{-1} was only noticeable in the (111) orientation (Figure 1 and Tables 1 and S1). Besides, our Raman spectra displayed many low-intensity peaks at 50–200 cm^{-1}, which could possibly be associated with the fluorescence from the sample–laser interactions. Similar peaks were also observed in our other difluoride samples, and they maintained their frequencies even under high-pressure conditions (Figure S2). The Raman shift of the peaks at 292.9(1) and 405.6(1) cm^{-1} exhibits a monotonic increase
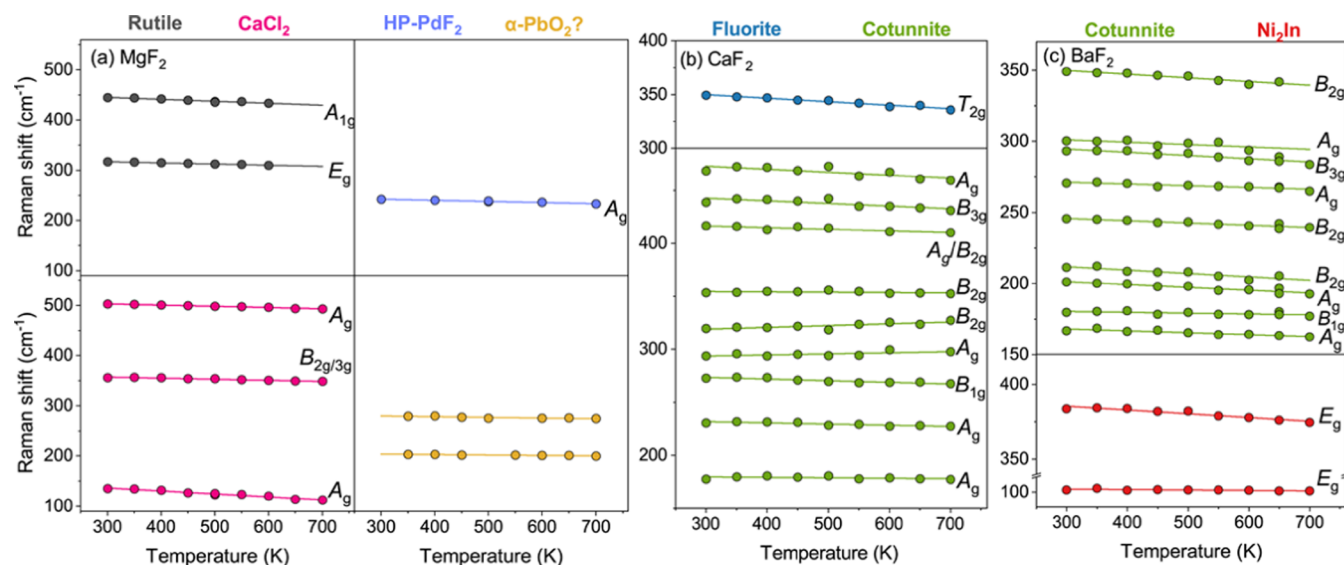
Figure 4. Temperature dependence of the Raman modes for difluorides at a given pressure. (a) MgF$_2$. The rutile-type phase at 5.4(1) GPa, CaCl$_2$- and α-PbO$_2$-type phases at 17.5(1) GPa, and the HP-PdF$_2$-type phase at 25.0(1) GPa; (b) CaF$_2$. The fluorite-type phase at 4.8(1) GPa and the cotunnite-type phase at 17.5(1) GPa. (c) BaF$_2$. The cotunnite-type phase at 4.8(1) GPa and the Ni$_2$In-type phase at 17.5(1) GPa. Solid circles: experimental data; lines: fitting results.

with pressure (Figure 2). The peak at 405.6(1) cm^{-1} can be observed up to 35.3(2) GPa, whereas the peak at 292.9(1) cm^{-1} disappeared at 26.0(2) GPa. The signal of the wide band at 511.2(6) cm^{-1} was under the detection limit at high pressures. We observed the appearance of a new peak at 58(1) cm^{-1} at 9.9(2) GPa, but it disappeared at 36.8(2) GPa. Another notable change was observed at 21.0(2) GPa, marked by the appearance of a new peak at 236(1) cm^{-1}. Two more peaks at 325.4(5) and 400.3(7) cm^{-1} appeared successively at ~30 GPa. The Raman shifts of these three peaks increased to 265.4(2), 345.8(6), and 429.6(7) cm^{-1} at 38.5(1) GPa. The behavior upon decompression from 38.5(1) GPa is very different with compression, as the Raman shifts of three peaks at 265.4(2), 345.8(6), and 429.6(7) cm^{-1} at 38.5(1) GPa exhibited a linear decrease to 213.8(4), 268(2), and 331(3) cm^{-1} at 10.0(1) GPa, respectively (Figure S3). Both peaks at 213.8(4) and 331(3) cm^{-1} disappear upon further decompression with the appearance of a new peak at 192.0(4) cm^{-1} (Figure S3). When decompressed to ~4 GPa, we observed the presence of two new peaks, the Raman shifts of which decreased to 292(1) and 406(1) cm^{-1} at 1 bar, respectively.

To explore the combined effect of pressure and temperature on the phase diagram of MgF$_2$, we collected Raman spectra up to 35 GPa and 700 K (Figures 3 and S4). Raman shifts for all of the active modes follow a linear decrease with temperature at a given pressure (Figure 4). In general, at high temperatures, MgF$_2$ follows the same transition sequence as it does at 300 K with increasing pressure. For example, a new peak at 58(1) cm^{-1} was observed at 9.9(2) GPa and 300 K, and it was present at a slightly higher pressure of 14.2(2) GPa at 700 K (Figures 3 and S4). The second major change in the Raman spectra of MgF$_2$ at 300 K occurs at 21.0(2) GPa, represented by the appearance of a new Raman peak at 236(1) cm^{-1}. This peak at high temperatures occurs at pressures nearly identical to those at 300 K. At 300 K and ~30 GPa, we observed two new Raman peaks at 325.4(5) and 400.3(7) cm^{-1}. However, at elevated temperatures, the pressures at which these two Raman peaks appear are slightly lower than at 300 K. For example, at

700 K, these two peaks were observed at ~27 GPa. In contrast to samples with other orientations, two new peaks at 200(1) and 275(1) cm^{-1}, which were never observed at 300 K, were present clearly at 400−700 K between 14.6(1) and 21(1) GPa in the (111) orientation (Figures 4 and S4). Both peaks disappeared at ~21 GPa at high temperatures.

In XRD measurements, we observed 5−14 reflections in the rutile-type phase of MgF$_2$ at high P−T conditions (Figure S5). At 300 K, the 101, 200, 210, 310, 301, 400, and 410 reflection spots split into pairs of reflection points of (101 and 011), (200 and 020), (210 and 120), (310 and 130), (301 and 031), (400 and 040), and (410 and 140) at 10.1(1) GPa, respectively. When the temperature was elevated to 600 K, these changes were observed at a slightly higher pressure of 12.1(1) GPa (Figures 5 and S5). We observed a dramatic change in the XRD pattern at 21.7−22.8(4) GPa for all of the investigated temperatures, marked by the transformation of reflection spots to lines and the occurrence of 4−8 new reflection lines (Figure S5), which indicates the transition between the CaCl$_2$ and HP-PdF$_2$ structures. At 300 K, two new additional peaks appeared at 44.2(1) GPa, and the number of the peaks gradually increased with pressure, suggesting the transition to the cotunnite structure. At 700 K, similar phenomena were observed at a slightly lower pressure of 42.7(3) GPa (Figure S5).

3.2. CaF$_2$. In the Raman spectra of CaF$_2$, a single peak at 323.0(1) cm^{-1} was observed under ambient conditions (Figures 1 and 2 and Tables 2 and S1). The Raman shift of this peak increases linearly with pressure up to 9.6(3) GPa, and the disappearance of this single peak accompanied by the appearance of 14 new peaks at 168−433(1) cm^{-1} was observed (Figures 1 and 2). Except for one peak present at 265 cm^{-1} at 9.6(3) GPa, the Raman shifts of all of the new peaks displayed a linear increase with pressure (Figures 1 and 2). During decompression from 39 GPa, these high-pressure peaks persisted down to 5 GPa (Figure S3). At high temperatures, increasing the pressure leads to a similar change in the Raman spectra of CaF$_2$ at 300 K (Figures 3, 4, and S4).
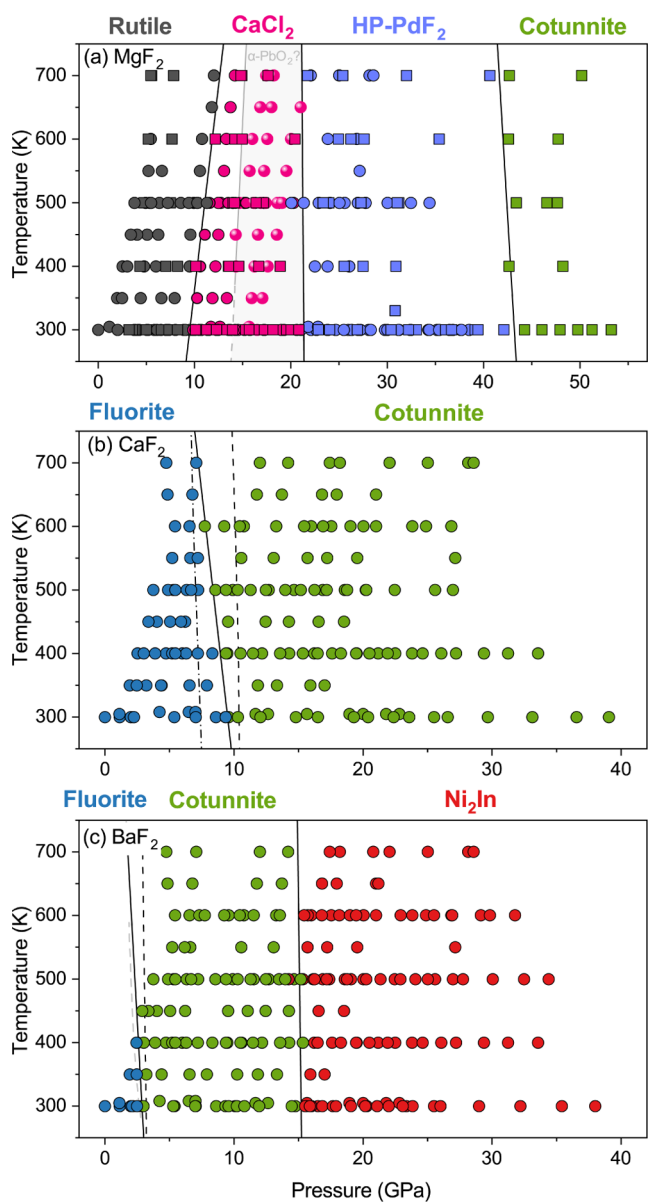
Figure 5. High $P-T$ phase diagrams of MgF$_2$, CaF$_2$, and BaF$_2$. (a) MgF$_2$. Black: rutile-type phase; pink: CaCl$_2$-type phase; purple: HP-PdF$_2$-type phase; green: cotunnite-type phase; solid circles: Raman results; solid squares: XRD results; solid circles with white dots: the mixture of CaCl$_2$- and α-PbO$_2$-type phases. (b) CaF$_2$. Blue: fluorite-type phase; green: cotunnite-type phase; black dashed lines: the calculated phase boundary from Cazorla and Errandonea;[31] black dotted dashed lines: the calculated phase boundary from Nelson et al.[30] (c) BaF$_2$. Blue: fluorite-type phase; green: cotunnite-type phase; red: Ni$_2$In-type phase; gray dashed lines: experimentally determined phase boundary from Samara;[41] black dashed lines: the calculated phase boundary from Cazorla et al.[38] Black and gray solid lines: phase boundary determined in this study.

However, the change in Raman spectra occurred at a slightly lower pressure than that at 300 K. For example, we observed the presence of 13 new peaks at 7.8(2) GPa and 600 K compared to 9.6(3) GPa and 300 K.

3.3. BaF$_2$. There was only one active Raman mode observed at 240.9(1) cm^{-1} at ambient conditions for BaF$_2$ (Figures 1 and 2 and Tables 3 and S1). The Raman shift of this peak increased linearly with pressures up to 3 GPa. A distinct change was observed at 3.0(3) GPa, with the disappearance of

Table 2. Raman Frequencies ν (cm^{-1}), First-Order Pressure Coefficients dν/dp (cm^{-1}/GPa), and Mode Grüneisen Parameter γ of the Fluorite- (1 bar) and Cotunnite-Type Phases (10.1 GPa) of CaF$_2$ at 300 K[a]

phase	mode symmetry	ν	ν_0 (fit)	dν/dp	γ_i
fluorite (1 bar)	T$_{2g}$	323.0(1)	322.7(5)	5.26(9)	1.32
cotunnite (10.1 GPa)	B$_{3g}$	168.4(8)	152(2)	1.11(5)	0.81
	A$_g$	168.4(8)	147(1)	1.8(1)	1.34
	B$_{1g}$	184(1)	163(1)	1.5(6)	1.22
	A$_g$	223.6(5)	215.2(7)	0.79(5)	0.48
	B$_{1g}$	255(1)	230(2)	2.5(1)	1.12
	A$_g$	273.1(9)	255(4)	2.3(5)	0.94
	B$_{2g}$	294(1)	276(1)	3.1(7)	0.77
	B$_{2g}$	318.8(4)	315.5(5)	0.34(4)	0.10
	B$_{2g}$	345.2(3)	338(1)	0.86(6)	0.27
	A$_g$	397.2(9)	385(1)	1.54(3)	0.44
	B$_{2g}$	397.2(9)	365(2)	3.0(1)	0.88
	B$_{3g}$	413(1)	375(2)	4.0(1)	1.07
	A$_g$	433.4(7)	389(2)	4.7(3)	1.21

[a]The fitting values of zero-pressure frequency are also displayed for different modes.

Table 3. Raman Frequencies ν (cm^{-1}), First-Order Pressure Coefficients dν/dp (cm^{-1}/GPa), and Mode Grüneisen Parameter γ of the Fluorite- (1 bar), Cotunnite- (6.3 GPa), and Ni$_2$In-Type Phases (15.5 GPa) of BaF$_2$ at 300 K[a]

phase	mode symmetry	ν	ν_0 (fit)	dν/dp	γ_i
fluorite (1 bar)	T$_{2g}$	240.9(1)	242.2(6)	6.2(3)	1.45
cotunnite (6.3 GPa)	A$_g$	170.2(4)	158(1)	1.8(2)	0.83
	B$_{1g}$	186.2(7)	163(1)	3.5(1)	1.47
	A$_g$	205.0(7)	189(1)	2.5(1)	0.94
	B$_{2g}$	219(2)	192(3)	4.0(3)	1.44
	B$_{2g}$	249.7(2)	234.4(7)	2.34(6)	0.74
	A$_g$	275.7(4)	256(1)	3.0(2)	0.87
	B$_{3g}$	300.3(2)	270(1)	4.9(1)	1.29
	A$_g$	310(1)	274(1)	5.5(1)	1.40
	B$_{2g}$	357(1)	324(4)	5.2(4)	1.14
Ni$_2$In (15.5 GPa)	E$_g$	101.1(1)	93(1)	0.48(5)	0.63
	E$_g$	379.6(1)	332(1)	2.98(6)	1.04

[a]The fitting values of zero-pressure frequency are also displayed for different modes.

the single peak and the appearance of the nine new peaks at 166−348(2) cm^{-1} (Figure 2). The Raman shifts of all nine peaks increase with increasing pressure. Another significant change occurred at 15.5(4) GPa, characterized by the appearance of two new peaks at 101.1(1) and 379.6(1) cm^{-1} and an apparent softening in the Raman shift of one peak previously observed at 163.1(4) cm^{-1} at ~3 GPa (Figure 2). Meanwhile, the Raman modes previously observed at 3−15 GPa either transform into three wide peaks at ~220, 270, and 350 cm^{-1} or gradually decrease in intensity until they completely disappear at ~20 GPa (Figures 1 and 2). The Raman shifts of the peaks at 101.1(1) and 379.6(1) cm^{-1} exhibit a linear increase with pressure up to 39 GPa. Upon decompression from 39 GPa, these two peaks were observed down to 12 GPa, whereas nine new peaks at 159−371(2) cm^{-1} gradually occurred at 10−15 GPa (Figure S3). When the pressure inside the DAC is completely released, the Raman spectrum of BaF$_2$ returned to having only one peak at 241

cm^{-1} under ambient conditions. Under high $P-T$ conditions, the change of the Raman spectra of BaF_2 was similar to that at 300 K and high pressure (Figures 3, 4, and S4). The first change was characterized by the disappearance of the single peak at 241 cm^{-1} and occurred at slightly lower pressures with increasing temperature. The second major change in Raman spectra occurred at 15 GPa, independent of the temperature.

4. DISCUSSION

4.1. Phase Transition of MgF$_2$ at High $P-T$. According to the group theory, the rutile-type structure of difluorides exhibits four Raman-active modes (B_{1g}, E_g, A_{1g}, B_{2g}).[16] At ambient conditions, the observed peaks of MgF_2 at 292.9(1), 405.6(1), and 511.2(6) cm^{-1} correspond to E_g, A_{1g}, and B_{2g} modes, respectively (Table S1).[18] Previous XRD measurements and theoretical studies have revealed that MgF_2 undergoes a second-order ferroelastic transition to the $CaCl_2$-type phase at 4.8−12.3 GPa and 300 K.[10,23,25−27,30,52,54,55] According to the Landau theory, the transition pressure from rutile to the $CaCl_2$-type phase could be determined by the intersection of squared Raman shifts of B_{1g} and A_g modes.[56,57] In this study, although the fluorescence peaks within the range of 50−200 cm^{-1} partly impede the detection of the B_{1g} mode in the rutile-type phase, the A_g mode in the $CaCl_2$-type structure has a much greater intensity than the fluorescence peaks and was present at 58(1) cm^{-1} at 9.9(2) GPa (Figures 1 and S3). We observed the splitting of the refraction spots at 10.1(1) GPa in the collected diffraction patterns (Figures 5 and S5). The transition pressure could also be determined by the intersection of the linear extrapolation of a straight line of the squared symmetry-breaking strains from the lattice parameters $(e_1-e_2)^2$ and the pressure axis (Figure S6 and Table S2).[56,58] This yields a transition pressure of 8.6(2) GPa and 300 K, consistent with our Raman results.[10]

Previous results have shown that the $CaCl_2$- to HP-PdF$_2$-type phase transition of MgF_2 occurs at 13.5−15.4 GPa, and the HP-PdF$_2$-type phase has five Raman-active modes ($E_g + A_g + 3T_g$).[10,25,30,52] However, there is no new peak or other noticeable change in our Raman spectra until 21.0(2) GPa. Since MgF_2 and ZnF_2 have the same transition sequence, here, we assign the observed modes based on the findings from ZnF_2.[3,4] The new peak emerged at 21.0(2) GPa from the HP-PdF$_2$-type phase with a Raman shift of 236(1) cm^{-1}, which is consistent with the strongest A_g mode. The other modes, originally expected to occur with the A_g mode, exhibited delayed appearances due to their weak intensities. Both T_g and E_g modes became detectable at pressures as high as 30 GPa, while the other two modes remained undetected. Meanwhile, we observed a dramatic change in the diffraction pattern of MgF_2 at 22.8(4) GPa. This change in the XRD pattern should be caused by the $CaCl_2$- to HP-PdF$_2$-type phase transition and occurred at a slightly higher pressure than that observed in Raman measurements. All of the diffraction lines can be well indexed into a cubic unit cell of the HP-PdF$_2$-type structure (Figure S5).[10] Although our Raman measurements indicate no additional changes up to 38.5(1) GPa, two additional peaks were observed at 44.2(2) GPa in our XRD pattern, which should be related to the transition to the cotunnite structure.

The observed transition pressures between the $CaCl_2$ and HP-PdF$_2$ structures (21 GPa) and between the HP-PdF$_2$ and cotunnite structures (44 GPa) are higher than previous experimental results (14 and 38 GPa), which used powder samples in XRD measurements (Figure 6).[10] The difference in
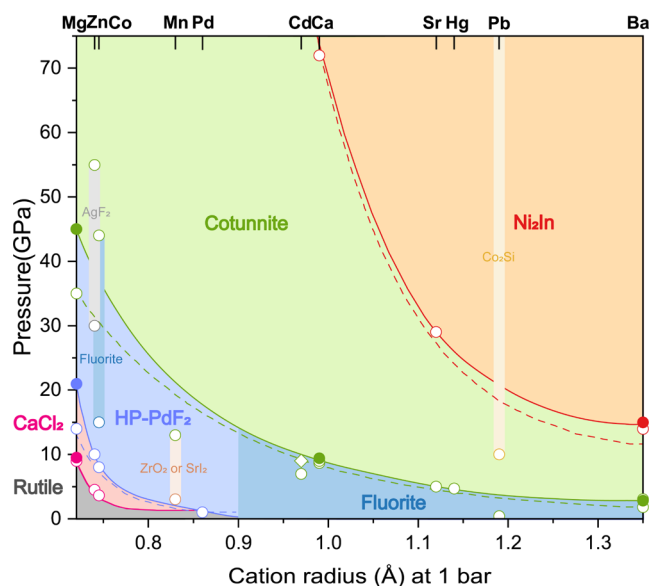

Figure 6. Relationship between the phase transition pressures and cation radii for difluorides at 300 K. Solid circles: results from this study; open circles: results from previous experiments;[3−5,7,9−12,22] open diamonds: results from theoretical calculation;[61] solid lines: phase boundary determined based on our results and those from the literature; dashed lines: phase boundary determined by Dorfman et al.[5]

the transition pressure between this study and previous experimental results might be attributed to the choice of the pressure medium and the morphology of the samples. Previous experimental studies used powder MgF_2 samples and a methanol−ethanol−water (MEW) mixture as the pressure medium.[10] Compared to Ar or Ne used in this study, MEW remains hydrostatic within 10 GPa but develops a large pressure gradient and deviatoric stress with increasing pressure.[59] Meanwhile, numerous crystal defects exist between individual grain boundaries in the powder samples. As the magnitude of deviatoric and micro stress increases with pressure, the transition pressure shifts to lower pressures.[60] These explain the relatively low transition pressures of powder MgF_2 samples from $CaCl_2$ to the HP-PdF$_2$ structure and subsequently to the cotunnite structure while using MEW as the pressure medium.

In our spectra upon decompression from 38.5(1) GPa, two new peaks at 192.0(4) and 268(2) cm^{-1} at 10.8(2) GPa occurred along with two weak peaks trailing the positions of the rutile-type phase, representing the emergence of a new structure (Figure S3). Previous XRD experiments reported that HP-PdF$_2$-type MgF_2 and other AX_2 compounds such as ZnF_2 and SnO_2 were transformed into a mixture of rutile- and α-PbO_2-type phases upon decompression.[10,14,42] The mixture arose from the competition between the formation of rutile- and α-PbO_2-type materials, with the latter serving as a unit-cell twin of the rutile phase.[10,14] Nevertheless, we detected only two previously unknown peaks below 12 GPa. As we lack sufficient evidence to definitively attribute these two peaks, we tentatively associate them with the α-PbO_2-type phase. This assumption is based on the similarity in the relative positions and slopes of these Raman-active modes with the only two strong peaks below 300 cm^{-1} observed in the α-PbO_2-type phase of TiO_2 and MnF_2 (Table S3).[17,62,63] Consequently, we propose that MgF_2 maintains its HP-PdF$_2$-type polymorph

down to 12 GPa and transforms into a mixture of rutile and α-PbO_2-type phases upon decompression from 38.5 GPa.

The high $P-T$ phase diagram of MgF_2 by combining Raman and XRD results is plotted in Figure 5. The transition pressures from rutile to the $CaCl_2$ structure are 11.5(1) and 14.2(1) GPa at 500 and 700 K, respectively, which are higher than that at 300 K. The Clapeyron slope of the boundary between the rutile and $CaCl_2$ structures was determined to be 8.7(9) MPa/K. The next dramatic change characterized by the occurrence of A_g mode and new peaks in XRD spectra indicated that the phase transition from $CaCl_2$ to the HP-PdF_2 structure occurred at 21(1) GPa at both 500 and 700 K. The impact of temperature on this boundary was very small, with a Clapeyron slope approaching $-0.3(3)$ MPa/K. The new peaks encompassing all those observed at room temperature and those reported by Haines et al.[10] for the cotunnite structure in our XRD spectra indicated that the transformation from HP-PdF_2 to the cotunnite structure occurred at 43.4(3) and 42.7(3) GPa for 500 and 700 K (Figure S5). Therefore, the Clapeyron slope between the boundary between HP-PdF_2 and cotunnite structures was negative ($-3.8(3)$ MPa/K). Notably, a similar transition sequence has been reported for SiO_2 based on experimental and theoretical studies, the Clapeyron slopes of which are 5.8−20 MPa/K for the rutile-to-$CaCl_2$ transition, 0 MPa/K for the α-PbO_2-to-HP-PdF_2 transition, and a negative value for the HP-PdF_2-to-cotunnite transition.[30,38,64−70] As a low-pressure analogue of SiO_2, the Clapeyron slopes observed in this study for MgF_2 are very similar to those reported for SiO_2.[30,38,64−70]

Another particular issue is the α-PbO_2-type phase in AX_2-type compounds. As discussed by Haines and Léger,[14] it is more difficult for the $CaCl_2$ structure in AX_2-type compounds to transform into the α-PbO_2 structure than the HP-PdF_2 phase at ambient temperature because the former requires more significant activation energy to induce large structure changes. So far, the transformation from $CaCl_2$ to the α-PbO_2 structure in dioxides during compression has only occurred under nonhydrostatic conditions (i.e., SnO_2) or after laser heating (i.e., SiO_2 and GeO_2).[14,71−73] Similarly, this phenomenon has also been observed in difluorides.[43] Different from the transition sequence at 300 K, the $CaCl_2$-type MgF_2 was previously observed to partially transition into the α-PbO_2-type phase at 13.0 GPa and 600 °C using XRD in a large-volume press.[43] Between 14.6(1) and 21.0(1) GPa above 400 K, we observed the presence of two additional new peaks at 200 and 274 cm^{-1} in our collected Raman spectra for the samples with (111) orientation, coexisting with the peaks of the $CaCl_2$-type phase (Figures 3 and S7). These two peaks closely resembled those observed below 11 GPa during decompression, suggesting their association with the α-PbO_2-type phase. We thus suggest that the mixture of α-PbO_2- and $CaCl_2$-type phases may exist between 14.6(1) and 21.0(1) GPa at 400−700 K. The coexistence of the α-PbO_2- and $CaCl_2$-type phases was not observed in the Raman measurements for the samples with other orientations, indicating that the α-PbO_2-type phase of MgF_2 may be easier to be present along a certain orientation. However, the reason why the α-PbO_2-type phase was not observed in the XRD pattern may be due to the limited temperature holding time before measurements began. On account of the insufficient heating, the change of free energy is relatively low, which makes it difficult for MgF_2 to cross the energy barrier and enter the α-PbO_2-type phase.

4.2. Phase Transition of CaF_2 at High $P-T$. According to the group theory, only one mode (T_{2g}) is Raman-active in the fluorite-type structure for CaF_2, which is the peak at 323.0(1) cm^{-1} at ambient conditions. Previous experimental studies indicated that at 300 K, fluorite-type CaF_2 transforms to the cotunnite structure at 8.7−9.3 GPa.[5,34] 13 new peaks occurred at 9.6(3) GPa in our spectra, indicating the transformation of CaF_2 from the fluorite- to cotunnite-type phase, which is in agreement with previous experimental results.[5,34] According to recent computational results, there are 18 Raman-active modes ($6A_g$, $3B_{1g}$, $6B_{2g}$, $3B_{3g}$) in the cotunnite-type phase (Figures 1 and 2).[53,74] The observed 13 peaks at 168−433(1) cm^{-1} at 9.6−39 GPa are related to 13 modes ($5A_g$, $2B_{1g}$, $4B_{2g}$, $2B_{3g}$) among them. The peak at ∼265 cm^{-1} at 9.6(3) GPa, which exhibits downward dependence with pressure, is not the Raman-active mode of CaF_2 but is possibly due to the influence of fluorescence (Figures 1 and 2). With the elevating pressure, there was no significant change in our Raman spectra up to 39 GPa. This is also consistent with previous XRD results, which have shown that the next phase transition of CaF_2 occurs at 72 GPa upon laser heating.[5] High $P-T$ results allow us to determine the Clapeyron slope between the fluorite and cotunnite phases to be $-6.6(3)$ MPa/K, showing a much stronger temperature dependence than that predicted by previous theoretical studies.[30,38,69,70]

4.3. Phase Transition of BaF_2 at High $P-T$. Similar to CaF_2, the only peak of BaF_2 at 240.9(1) cm^{-1} at 1 bar is the T_{2g} mode. The presence of nine new peaks at 3.0(3) GPa indicated the transition to a cotunnite-type phase. The transition pressure from fluorite to the cotunnite structure determined in our study is consistent with previous results (3−3.2 GPa).[5,36] The observed nine peaks correspond to $4A_g$, B_{1g}, $3B_{2g}$, and B_{3g} modes in the cotunnite structure.[53] Softening of the A_g mode at 15.5(4) GPa together with the presence of two new peaks indicates the transition to the Ni_2In structure, consistent with literature results.[5,36] Two peaks above 15 GPa are E_g modes in the Ni_2In structure. Three wide peaks at ∼220, 270, and 350 cm^{-1} belonging to the cotunnite-type phase persisted until 20 GPa before completely disappearing. This could be caused by the energy barrier between these two phases.[75] At high $P-T$ conditions, the Clapeyron slope between the fluorite and cotunnite structures of BaF_2 was determined to be $-2.4(7)$ MPa/K, showing a stronger temperature dependence for this phase transition than the previous predicted value of -0.6 MPa/K from the theoretical study but in good agreement with the experimental results.[38,41] In contrast, the phase transition from cotunnite to the Ni_2In structure is weakly dependent on temperature, with a small Clapeyron slope of 0.3(3) MPa/K.

The above discussion shows that the phase transition of difluorides strongly depends on pressure, temperature, atomic radius, and electronic properties. In Figure 7, we plot the phase transition sequence of different difluorides at high $P-T$ conditions with varying atomic radii. Only our results and the theoretical results are included due to the lack of experimental results of other difluorides at high temperatures.[31,38] In general, our experimental results indicate that elevating the temperature can increase the transition pressure between rutile and $CaCl_2$ structures for difluorides with small cation radii such as MgF_2. However, the effect of the temperature on the $CaCl_2$- to HP-PdF_2-type phase transition pressure is negligible. On the other hand, regardless of the cation radius, the phase transition pressure from HP-PdF_2 and
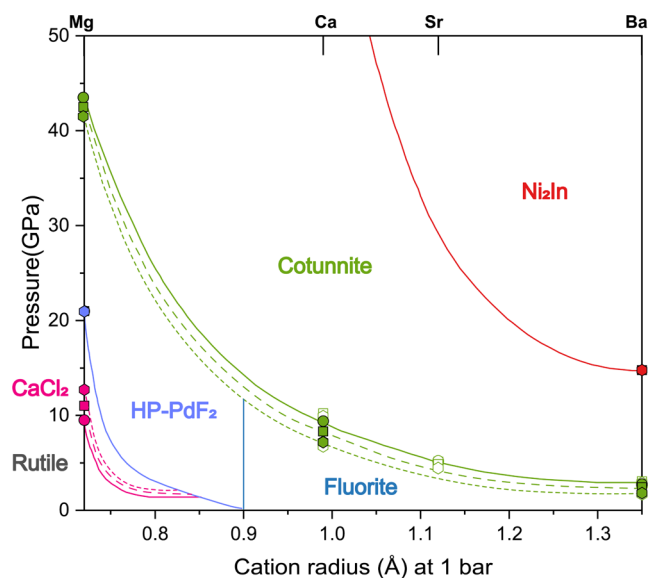
Figure 7. Relationship between the phase transition pressures and cation radii for difluorides at high $P-T$ conditions. Circles and solid lines: 300 K; squares and dashed lines: 500 K; hexagons and dotted lines: 700 K; solid symbols: results in our study; open symbols: results from previous studies; lines: phase boundary at different temperatures.[30,38,40,41]

fluorite to the cotunnite structure exhibits a negative dependence on temperature. For BaF_2 with a large cation radius, the transition pressure from cotunnite to the Ni_2In structure is also not sensitive to temperature.

4.4. Mode Grüneisen Parameters. The Grüneisen parameter is a numerical parameter that elucidates the impact of pressure and chemical bonding among atoms on materials. It serves as a key factor in interpreting the thermoelastic behaviors of materials at high $P-T$ conditions. From the

obtained Raman frequency shifts with pressure, the isothermal mode Grüneisen parameters can be calculated as follows

$$\gamma_i = -\frac{\partial \ln \nu_i}{\partial \ln V} = -\frac{V}{\nu_i}\frac{d\nu_i}{dV} = \frac{K_T}{\nu_i}\frac{d\nu_i}{dp}$$

where ν_i is the ith mode of vibration of the lattice, V is the volume, and K_T is the isothermal bulk modulus for different phases at a given pressure. The values of ν at each pressure and $d\nu/dp$ of MgF_2, CaF_2, and BaF_2 are derived by fitting the high-pressure Raman data in this study using a polynomial function (Tables 1−3). K_{T0} of rutile-type MgF_2 is derived from our XRD results with a fixed pressure derivative of $K_{T0}' = 4$, while that of fluorite-type CaF_2 and BaF_2 is from the experimental data of Dorfman et al.[5] (Tables S2 and S4). The ν_{i0}, $d\nu/dp$, and K_{T0} of other typical rutile- and fluorite-type AX_2 compounds are from previous Raman and XRD measurements (Table S4).[3,9,12,18,76,77] Since some dioxides crystallize as rutile-type structures at ambient conditions, we also compare the γ_{i0} of rutile-type difluorides with these dioxides (Table S4).[16,18,78−80] O^{2-} and F^- have different ionic radii. Here, we use the normalized ratio of cation radius/anion radius to eliminate the influence of the anion.

We first investigate the effect of the radius and d electrons on the mode Grüneisen parameters of Raman-active modes under ambient conditions. Our results show that the γ_{i0} values of the Raman-active modes of MgF_2, CaF_2, and BaF_2 are between 1 and 2 (Figure 8 and Tables 1−3). Except for ZnF_2, the γ_0 values of E_g, A_{1g}, and B_{2g} modes for rutile-type difluorides exhibit a linear increase with increasing cation radius, while the B_{1g} mode has a negative γ_0, which decreases with cation radius. For fluorite-type difluorides, the γ_0 of the F_{2g} mode exhibits a positive but weaker dependence on the cation radius. Compared to dioxides, the absolute values of the γ_0 of difluorides are larger, and γ_0 values of A_{1g}, E_g, and B_{1g} modes show a stronger dependence on the cation radius. Ignoring the transition metal compounds TiO_2 and RuO_2, increasing the cation radius leads to the same linear increase in
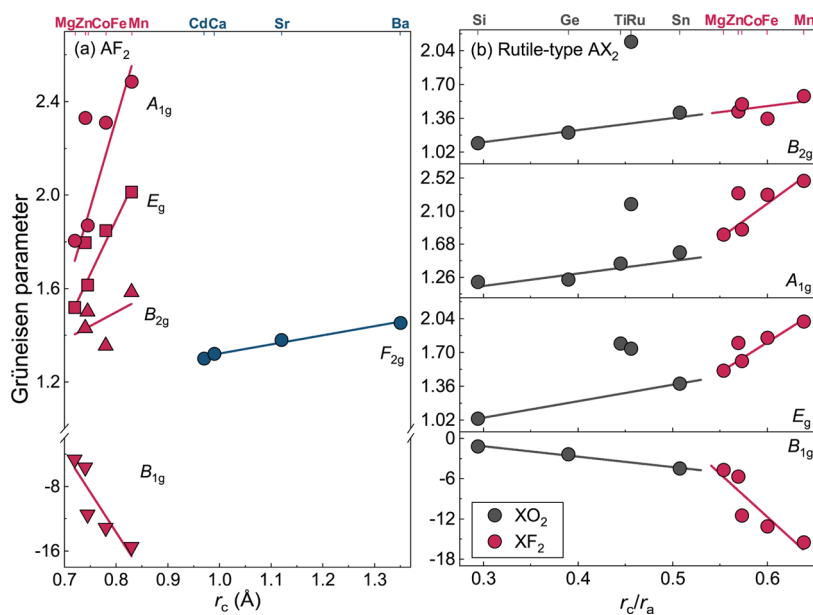

Figure 8. Mode Grüneisen parameters of typical difluorides and dioxides: (a) difluorides and (b) rutile-type dioxides and difluorides. The data for dioxides and difluorides were calculated from the experimental and theoretical calculations using the bulk modulus summarized in Table S4.[3,9,16,18,28,62,76−80,82] Solid lines represent least-squares fits to the data.
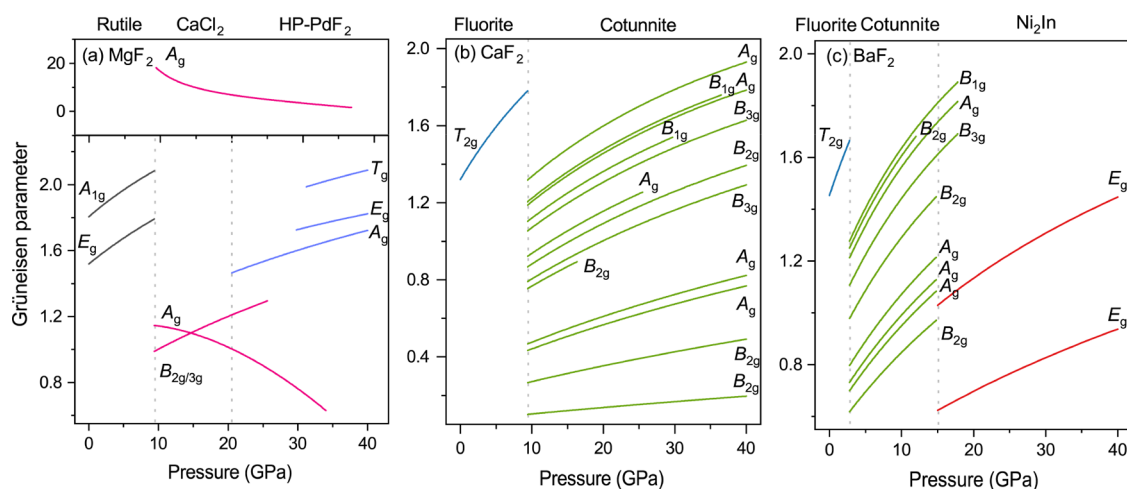
Figure 9. Mode Grüneisen parameters for the high-pressure phases of difluorides at 300 K. (a) MgF_2. (b) CaF_2. (c) BaF_2. Gray dotted lines: the phase boundary of different phases.

the γ_0 of the B_{2g} mode for difluorides and dioxides. Either difluorides or dioxides with transition metals as cations have the γ_0 value that deviates from the general trend, which may be related to the d electron of the cation or the presence of magneto-elastic coupling.[81]

We only calculate the Grüneisen parameters at high pressures for MgF_2, CaF_2, and BaF_2 due to a lack of experimental constraints on other difluorides (Figure 9 and Tables 1−3). Using our XRD data of MgF_2 at high pressures, we derived $K_{T0} = 82(3)$ and $119(4)$ GPa for the $CaCl_2$- and HP-PdF_2-type phases with a fixed K_{T0}' of 4, respectively (Table S4). Bulk modulus values for the high-pressure phases of CaF_2 and BaF_2 were calculated using the equation of state from a previous experimental study.[5] Our calculation shows that the mode γ values of MgF_2 in the rutile structure increase with pressure. Due to the instability of the structure around transformation and the influence of the B_{1g} mode, the γ value of the A_g mode that occurred at $58(1)$ cm^{-1} at $9.9(2)$ GPa of the $CaCl_2$ structure is 10−20 larger than those of other modes and shows a highly nonlinear decrease with pressure to 2 at 35 GPa. Like this A_g mode, the γ of another A_g mode present at $472.3(1)$ cm^{-1} and $9.9(2)$ GPa also shows a downward trend. In contrast, the mode γ values of all of the other high-pressure phases for MgF_2, CaF_2, and BaF_2 increase with pressure.

5. CONCLUSIONS

To constrain the combined effect of pressure, temperature, and radius on the phase transition of AF_2 difluorides, we perform a series of Raman and XRD measurements for single-crystal MgF_2, CaF_2, and BaF_2 up to 55 GPa and 700 K. The rutile structure MgF_2 with a small cationic radius transitions to $CaCl_2$ structure at $9.9(1)$ GPa, consistent with previous studies. However, the transition pressures to HP-PdF_2 structure at $21.0(2)$ GPa and the cotunnite structure at $44.2(2)$ GPa are greater than previous experimental results using polycrystalline samples. The difference in the transition pressure could be caused by using a less hydrostatic pressure medium above 10 GPa in previous study and the physical forms of the samples. Experiments at high $P-T$ reveal that these three phase transitions have very different Clapeyron slopes: $8.7(9)$ MPa/K for the rutile-$CaCl_2$ phase transition, $−0.3(3)$ MPa/K for the $CaCl_2$−HP-PdF_2 phase transition, and $−3.8(3)$ MPa/K for the HP-PdF_2-cotunnite phase transition. Meanwhile, our study has

also shown that the increase in temperature may help to lower the energy barrier from the $CaCl_2$- to α-PbO_2-type phase and allow the latter one to appear above 400 K in some specific crystallographic orientations, such as (111). Difluorides, CaF_2 and BaF_2, with larger cationic radii transition from fluorite to the cotunnite structure at $9.6(3)$ and $3.0(3)$ GPa at 300 K, respectively, and BaF_2 will further transform to the Ni_2In-type phase at $15.5(4)$ GPa. Although elevating temperature causes a lower transition pressure from fluorite to the cotunnite-type phase for both CaF_2 and BaF_2, it hardly changes the transition pressure from cotunnite to the Ni_2In structure for BaF_2. We further calculated the mode Grüneisen parameters for difluorides and dioxides to decipher the influence of cationic radius on these important parameters. The increase of the cationic radius causes a linear increase in the Grüneisen parameters for difluorides and dioxides, except for the ones with transition metals as cations. Our results are important for understanding the transition sequence and vibrational properties of AX_2-type minerals.

■ ASSOCIATED CONTENT

Ⓢ Supporting Information

The Supporting Information is available free of charge at https://pubs.acs.org/doi/10.1021/acsomega.4c01347.

Additional experiment details and materials, including photographs of the experimental setup (Figures S1−S7 and Tables S1−S4) (PDF)

■ AUTHOR INFORMATION

Corresponding Author

Ningyu Sun − *Deep Space Exploration Laboratory/School of Earth and Space Sciences, University of Science and Technology of China, Hefei 230026, China; CAS Center for Excellence in Comparative Planetology and Frontiers Science Center for Planetary Exploration and Emerging Technologies, University of Science and Technology of China, Hefei 230026, China;* ⓞ orcid.org/0000-0002-8723-9529; Email: ningyu@ustc.edu.cn

Authors

Xinyue Zhang − *Deep Space Exploration Laboratory/School of Earth and Space Sciences, University of Science and Technology of China, Hefei 230026, China*

Luo Li − *Deep Space Exploration Laboratory/School of Earth and Space Sciences, University of Science and Technology of China, Hefei 230026, China*

Yingxin Yu − *Deep Space Exploration Laboratory/School of Earth and Space Sciences, University of Science and Technology of China, Hefei 230026, China*

Qingchun Zhang − *Deep Space Exploration Laboratory/School of Earth and Space Sciences, University of Science and Technology of China, Hefei 230026, China*

Zhu Mao − *Deep Space Exploration Laboratory/School of Earth and Space Sciences, University of Science and Technology of China, Hefei 230026, China; CAS Center for Excellence in Comparative Planetology and Frontiers Science Center for Planetary Exploration and Emerging Technologies, University of Science and Technology of China, Hefei 230026, China*

Dongzhou Zhang − *GeoSoilEnviroCARS, University of Chicago, Argonne, Illinois 60439, United States*

Complete contact information is available at:
https://pubs.acs.org/10.1021/acsomega.4c01347

Notes

The authors declare no competing financial interest.

■ REFERENCES

(1) Massa, W. Fluorides: Solid-State Chemistry. In *Encyclopedia of Inorganic Chemistry*; John Wiley & Sons Inc., 2006.

(2) Cotter, T. M.; Thomas, M. E.; Tropf, W. J. Magnesium Fluoride (MgF_2). In *Handbook of Optical Constants of Solids*; Harcourt Brace Jovanovich, 1998; pp 899−918.

(3) Barreda-Argüeso, J. A.; López-Moreno, S.; Sanz-Ortiz, M. N.; et al. Pressure-induced phase-transition sequence in CoF_2: An experimental and first-principles study on the crystal, vibrational, and electronic properties. *Phys. Rev. B* **2013**, *88*, No. 214108.

(4) Kurzydłowski, D.; Oleksiak, A.; Pillai, S. B.; Jha, P. K. High-Pressure Phase Transitions of Zinc Difluoride up to 55 GPa. *Inorg. Chem.* **2020**, *59*, 2584−2593.

(5) Dorfman, S. M.; Jiang, F.; Mao, Z.; Kubo, A.; Meng, Y.; Prakapenka, V. B.; Duffy, T. S. Phase transitions and equations of state of alkaline earth fluorides CaF_2, SrF_2, and BaF_2 to Mbar pressures. *Phys. Rev. B* **2010**, *81*, No. 174121.

(6) Pauling, L. The sizes of ions and the structure of ionic crystals. *J. Am. Chem. Soc.* **1927**, *49*, 765−790.

(7) Schyck, S.; Evlyukhin, E.; Kim, E.; Pravica, M. High pressure behavior of mercury difluoride (HgF_2). *Chem. Phys. Lett.* **2019**, *724*, 35−41.

(8) Oberschmidt, J.; Lazarus, D. Ionic conductivity, activation volumes, and high-pressure phase transitions in PbF_2 and $SrCl_2$. *Phys. Rev. B* **1980**, *21*, No. 2952.

(9) Liu, G.; Wang, H.; Ma, Y.; Ma, Y. Phase transition of cadmium fluoride under high pressure. *Solid State Commun.* **2011**, *151*, 1899−1902.

(10) Haines, J.; Léger, J. M.; Gorelli, F.; Klug, D. D.; Tse, J. S.; Li, Z. Q. X-ray diffraction and theoretical studies of the high-pressure structures and phase transitions in magnesium fluoride. *Phys. Rev. B* **2001**, *64*, No. 134110.

(11) Tressaud, A.; Soubeyroux, J. L.; Touhara, H.; Demazeau, G.; Langlais, F. On a new structural type of fluorine compounds: Crystal and magnetic structures of a high pressure form of PdF_2. *Mater. Res. Bull.* **1981**, *16*, 207−214.

(12) Stavrou, E.; Yao, Y.; Goncharov, A. F.; Konôpková, Z.; Raptis, C. High-pressure structural study of MnF_2. *Phys. Rev. B* **2016**, *93*, No. 054101.

(13) Haines, J.; Léger, J. M.; Schulte, O. The high-pressure phase transition sequence from the rutile-type through to the cotunnite-type structure in PbO_2. *J. Phys.: Condens. Matter* **1996**, *8*, 1631−1646.

(14) Haines, J.; Léger, J. M. X-ray diffraction study of the phase transitions and structural evolution of tin dioxide at high pressure: Relationships between structure types and implications for other rutile-type dioxides. *Phys. Rev. B* **1997**, *55*, No. 11144.

(15) Haines, J.; Lger, J. M.; Chateau, C.; Pereira, A. S. Structural evolution of rutile-type and $CaCl_2$-type germanium dioxide at high pressure. *Phys. Chem. Miner.* **2000**, *27*, 575−582.

(16) Kingma, K. J.; Cohen, R. E.; Hemley, R. J.; Mao, H.-k. Transformation of stishovite to a denser phase at lower-mantle pressures. *Nature* **1995**, *374*, 243−245.

(17) Lagarec, K.; Desgreniers, S. Raman study of single crystal anatase TiO_2 up to 70 GPa. *Solid State Commun.* **1995**, *94*, 519−524.

(18) Porto, S. P. S.; Fleury, P. A.; Damen, T. C. Raman Spectra of TiO_2, MgF_2, ZnF_2, FeF_2, and MnF_2. *Phys. Rev.* **1967**, *154*, No. 522.

(19) Jones, L. E. A.; Liebermann, R. C. Elastic and thermal properties of fluoride and oxide analogues in the rocksalt, fluorite, rutile and perovskite structures. *Phys. Earth Planet. Inter.* **1974**, *9*, 101−107.

(20) Zouboulis, I. S.; Jiang, F.; Wang, J.; Duffy, T. S. Single-crystal elastic constants of magnesium difluoride (MgF_2) to 7.4 GPa. *J. Phys. Chem. Solids* **2014**, *75*, 136−141.

(21) Duffy, T.; Madhusudhan, N.; Lee, K. K. M.Mineralogy of Super-Earth Planets. In *Treatise on Geophysics*; Elsevier, 2015; pp 149−178.

(22) Stan, C. V.; Dutta, R.; White, C. E.; Prakapenka, V.; Duffy, T. S. High-pressure polymorphism of PbF_2 to 75 GPa. *Phys. Rev. B* **2016**, *94*, No. 024104.

(23) Ocampo, I. K.; Winey, J. M.; Toyoda, Y.; Duffy, T. S. Dynamic compression of [100] MgF_2 single crystals: Shock-induced polymorphism to highly coordinated structures. *Phys. Rev. B* **2022**, *106*, No. 144108.

(24) Sneed, D. T.; Smith, G. A.; Kearney, J. S. C.; Childs, C.; Park, C.; Lawler, K. V.; Salamat, A.; Smith, D. Stable and metastable structures of tin (IV) oxide at high pressure. *Philos. Trans. R. Soc., A* **2023**, *381*, No. 20220346.

(25) Kanchana, V.; Vaitheeswaran, G.; Rajagopalan, M. High-pressure structural phase transitions in magnesium fluoride studied by electronic structure calculations. *J. Alloys Compd.* **2003**, *352*, 60−65.

(26) Öztürk, H.; Kürkçü, C.; Kürkçü, C. Structural phase transformations and new intermediate phases of MgF_2 under high-pressures applied via conjugate-gradient method. *J. Alloys Compd.* **2014**, *609*, 185−191.

(27) Öztürk, H.; Kürkçü, C.; Kürkçü, C. High-pressure structural phase transitions and intermediate phases of magnesium fluoride. *J. Alloys Compd.* **2014**, *597*, 155−160.

(28) Perakis, A.; Lampakis, D.; Boulmetis, Y. C.; Raptis, C. High-pressure Raman study of the ferroelastic rutile-to-$CaCl_2$ phase transition in ZnF_2. *Phys. Rev. B* **2005**, *72*, No. 144108.

(29) Ye, Z.; Li, B.; Chen, W.; Huang, S.; Xu, J.; Fan, D. Pressure-temperature phase diagram and thermoelastic behavior of manganese fluoride up to 13.1 GPa and 700 K. *Mater. Res. Express* **2019**, *6*, No. 116115.

(30) Nelson, J. R.; Needs, R. J.; Pickard, C. J. High-pressure phases of group-II difluorides: Polymorphism and superionicity. *Phys. Rev. B* **2017**, *95*, No. 054118.

(31) Cazorla, C.; Errandonea, D. Superionicity and polymorphism in calcium fluoride at high pressure. *Phys. Rev. Lett.* **2014**, *113*, No. 235902.

(32) Cazorla, C.; Errandonea, D. Comment on "High-pressure phases of group-II difluorides: Polymorphism and superionicity. *Phys. Rev. B* **2018**, *98*, No. 186101.

(33) Nelson, J. R.; Needs, R. J.; Pickard, C. J. Reply to "Comment on 'High-pressure phases of group-II difluorides: Polymorphism and superionicity. *Phys. Rev. B* **2018**, *98*, No. 186102.

(34) Speziale, S.; Duffy, T. S. Single-crystal elastic constants of fluorite (CaF_2) to 9.3 GPa. *Phys. Chem. Miner.* **2002**, *29*, 465−472.

(35) Leger, J. M.; Haines, J.; Atouf, A.; Schulte, O.; Hull, S. High-pressure x-ray- and neutron-diffraction studies of BaF_2: An example of a coordination number of 11 in AX_2 compounds. *Phys. Rev. B* **1995**, *52*, No. 13247.

(36) Smith, J. S.; Desgreniers, S.; Tse, J. S.; Sun, J.; Klug, D. D.; Ohishi, Y. High-pressure structures and vibrational spectra of barium fluoride: Results obtained under nearly hydrostatic conditions. *Phys. Rev. B* **2009**, *79*, No. 134104.

(37) Perakis, A.; Sarantopoulou, E.; Raptis, Y. S.; Raptis, C. Temperature dependence of Raman scattering and anharmonicity study of MgF_2. *Phys. Rev. B* **1999**, *59*, No. 775.

(38) Cazorla, C.; Sagotra, A. K.; King, M.; Errandonea, D. High-Pressure Phase Diagram and Superionicity of Alkaline Earth Metal Difluorides. *J. Phys. Chem. C* **2018**, *122*, 1267−1279.

(39) Mirwald, P. W.; Kennedy, G. C. The phase relations of calcium fluoride (fluorite) to 60 kbars and 1800°C. *J. Phys. Chem. Solids* **1978**, *39*, 859−861.

(40) Mirwald, P. W.; Kennedy, G. C. Phase relations for SrF_2 TO 50 Kbars and 1900°C and its compression to 40Kbars at 25°C. *J. Phys. Chem. Solids* **1980**, *41*, 1157−1160.

(41) Samara, G. A. Pressure-Induced Phase Transitions in Solids: BaF_2. *Phys. Rev. B* **1970**, *2*, No. 4194.

(42) Kusaba, K.; Kikegawa, T. In situ X-ray observation of phase transitions in under high pressure and high temperature. *Solid State Commun.* **2008**, *145*, 279−282.

(43) Kusaba, K.; Kikegawa, T. Stable phase with the α-PbO_2 type structure in under high pressure and high temperature. *Solid State Commun.* **2008**, *148*, 440−443.

(44) Mao, H. K.; Xu, J.; Bell, P. M. Calibration of the ruby pressure gauge to 800 kbar under quasi-hydrostatic conditions. *J. Geophys. Res.* **1986**, *91*, 4673−4676.

(45) Fei, Y.; Ricolleau, A.; Frank, M.; Mibe, K.; Shen, G.; Prakapenka, V. Toward an internally consistent pressure scale. *Proc. Natl. Acad. Sci. U.S.A.* **2007**, *104*, 9182−9186.

(46) Errandonea, D.; Boehler, R.; Japel, S.; Mezouar, M.; Benedetti, L. R. Structural transformation of compressed solid Ar: An x-ray diffraction study to114 GPa. *Phys. Rev. B* **2006**, *73*, No. 092106.

(47) Dewaele, A.; Datchi, F.; Loubeyre, P.; Mezouar, M. High pressure−high temperature equations of state of neon and diamond. *Phys. Rev. B* **2008**, *77*, No. 094106.

(48) Kantor, I.; Prakapenka, V.; Kantor, A.; Dera, P.; Kurnosov, A.; Sinogeikin, S.; Dubrovinskaia, N.; Dubrovinsky, L. BX90: A new diamond anvil cell design for X-ray diffraction and optical measurements. *Rev. Sci. Instrum.* **2012**, *83*, No. 125102.

(49) Datchi, F.; Dewaele, A.; Loubeyre, P.; Letoullec, R.; Le Godec, Y.; Canny, B. Optical pressure sensors for high-pressure−high-temperature studies in a diamond anvil cell. *High Pressure Res.* **2007**, *27*, 447−463.

(50) Zhang, D.; Dera, P. K.; Eng, P. J.; Stubbs, J. E.; Zhang, J. S.; Prakapenka, V. B.; Rivers, M. L. High Pressure Single Crystal Diffraction at PX∧2. *J. Visualized Exp.* **2017**, No. e54660.

(51) Zhang, L.-L.; Yan, S.; Jiang, S.; Yang, K.; Wang, H.; He, S.; Liang, D.-X.; Zhang, L.; He, Y.; Lan, X.-Y. Hard X-ray micro-focusing beamline at SSRF. *Nucl. Sci. Tech.* **2015**, *26*, No. 060101.

(52) Zhang, L.; Wang, Y.; Cui, T.; Ma, Y.; Zou, G. First-principles study of the pressure-induced rutile−$CaCl_2$ phase transition in MgF_2. *Solid State Commun.* **2008**, *145*, 283−287.

(53) Chernyshev, V. A.; Ryumshin, V. S.; Agzamova, P. A. Structure and Lattice Dynamics of MF_2 (M = Ca, Sr, Ba, Pb) in Cubic and Orthorhombic Phases: The ab initio Calculations. *Phys. Solid State* **2019**, *61*, 11−22.

(54) Ming, L.-c.; Manghnana, M. H. High pressure phase transformations in MgF_2 (rutile). *Geophys. Res. Lett.* **1979**, *6*, 13−16.

(55) Curetti, N.; Merli, M.; Capella, S.; Benna, P.; Pavese, A. Low-pressure ferroelastic phase transition in rutile-type AX_2 minerals: cassiterite (SnO_2), pyrolusite (MnO_2) and sellaite (MgF_2). *Phys. Chem. Miner.* **2019**, *46*, 987−1002.

(56) Carpenter, M. A.; Hemley, R. J.; Mao, H.-k. High-pressure elasticity of stishovite and the $P42/mnm \rightleftharpoons Pnnm$ phase transition. *J. Geophys. Res.: Solid Earth* **2000**, *105*, 10807−10816.

(57) Zhang, Y.; Fu, S.; Wang, B.; Lin, J. F. Elasticity of a pseudoproper ferroelastic transition from stishovite to post-stishovite at high pressure. *Phys. Rev. Lett.* **2021**, *126*, No. 025701.

(58) Buchen, J.; Marquardt, H.; Schulze, K.; Speziale, S.; Boffa Ballaran, T.; Nishiyama, N.; Hanfland, M. Equation of State of Polycrystalline Stishovite Across the Tetragonal-Orthorhombic Phase Transition. *J. Geophys. Res.: Solid Earth* **2018**, *123*, 7347−7360.

(59) Klotz, S.; Chervin, J. C.; Munsch, P.; Le Marchand, G. Hydrostatic limits of 11 pressure transmitting media. *J. Phys. D: Appl. Phys.* **2009**, *42*, No. 075413.

(60) Wang, B.; Buchen, J.; Méndez, A. S. J.; Kurnosov, A.; Criniti, G.; Liermann, H. P.; Marquardt, H. Strong Effect of Stress on the Seismic Signature of the Post-Stishovite Phase Transition in the Earth's Lower Mantle. *Geophys. Res. Lett.* **2023**, *50*, No. e2023GL102740.

(61) Wu, X.; Wu, Z. Theoretical calculations of the high-pressure phases of ZnF_2 and CdF_2. *Eur. Phys. J. B* **2006**, *50*, 521−526.

(62) López-Moreno, S.; Romero, A. H.; Mejia-Lopez, J.; Munoz, A. First-principles study of pressure-induced structural phase transitions in MnF_2. *Phys. Chem. Chem. Phys.* **2016**, *18*, 33250−33263.

(63) Cai, Y.; Zhang, C.; Feng, Y. P. Dielectric properties and lattice dynamics of α-PbO_2-type TiO_2: The role of soft phonon modes in pressure-induced phase transition to baddeleyite-type TiO_2. *Phys. Rev. B* **2011**, *84*, No. 094107.

(64) Ono, S.; Hirose, K.; Murakami, M.; Isshiki, M. Post-stishovite phase boundary in SiO_2 determined by in situ X-ray observations. *Earth Planet. Sci. Lett.* **2002**, *197*, 187−192.

(65) Bolfan-Casanova, N.; Andrault, D.; Amiguet, E.; Guignot, N. Equation of state and post-stishovite transformation of Al-bearing silica up to 100 GPa and 3000 K. *Phys. Earth Planet. Inter.* **2009**, *174*, 70−77.

(66) Tsuchiya, T.; Caracas, R.; Tsuchiya, J. First principles determination of the phase boundaries of high-pressure polymorphs of silica. *Geophys. Res. Lett.* **2004**, *31*, No. L11610.

(67) Oganov, A. R.; Gillan, M. J.; Price, G. D. Structural stability of silica at high pressures and temperatures. *Phys. Rev. B* **2005**, *71*, No. 064104.

(68) Kuwayama, Y.; Hirose, K.; Sata, N.; Ohishi, Y. The pyrite-type high-pressure form of silica. *Science* **2005**, *309*, 923−925.

(69) Tsuchiya, T.; Tsuchiya, J. Prediction of a hexagonal SiO_2 phase affecting stabilities of $MgSiO_3$ and $CaSiO_3$ at multimegabar pressures. *Proc. Natl. Acad. Sci. U.S.A.* **2011**, *108*, 1252−1255.

(70) Wu, S.; Umemoto, K.; Ji, M.; Wang, C.-Z.; Ho, K.-M.; Wentzcovitch, R. M. Identification of post-pyrite phase transitions in SiO_2 by a genetic algorithm. *Phys. Rev. B* **2011**, *83*, No. 184102.

(71) Prakapenka, V. B.; Dubrovinsky, L. S.; Shen, G.; Rivers, M. L.; Sutton, S. R.; Dmitriev, V.; Weber, H. P.; Le Bihan, T. α−PbO_2-type high-pressure polymorph of GeO_2. *Phys. Rev. B* **2003**, *67*, No. 132101.

(72) Murakami, M.; Hirose, K.; Ono, S.; Ohishi, Y. Stability of $CaCl_2$-type and α-PbO_2-type SiO_2 at high pressure and temperature

determined by in-situ X-ray measurements. *Geophys. Res. Lett.* **2003**, *30*, 11.

(73) Dutta, R.; White, C. E.; Greenberg, E.; Prakapenka, V. B.; Duffy, T. S. Equation of state of the $\alpha-PbO_2$ and $Pa\bar{3}$-type phases of GeO_2 to 120 GPa. *Phys. Rev. B* **2018**, *98*, No. 144106.

(74) Bazhenov, A. V.; Smirnova, I. S.; Fursova, T. N.; Maksimuk, M. Y.; Kulakov, A. B.; Bdikin, I. K. Optical phonon spectra of PbF_2 single crystals. *Phys. Solid State* **2000**, *42*, 41−50.

(75) Machon, D.; Le Bail, N.; Hermet, P.; Cornier, T.; Daniele, S.; Vignoli, S. Pressure-Induced Phase Transitions in TiO_2 Rutile Nanorods. *J. Phys. Chem. C* **2019**, *123*, 1948−1953.

(76) Kourouklis, G. A.; Anastassakis, E. Pressure-induced phase transitions and anharmonicity study of alkaline-earth fluorides. *Phys. Status Solidi (B)* **1989**, *152*, 89−99.

(77) López-Moreno, S.; Romero, A. H.; Mejía-López, J.; Muñoz, A.; Roshchin, I. V. First-principles study of electronic, vibrational, elastic, and magnetic properties of FeF_2 as a function of pressure. *Phys. Rev. B* **2012**, *85*, No. 134110.

(78) Haines, J.; Léger, J. M.; Chateau, C.; Bini, R.; Ulivi, L. Ferroelastic phase transition in rutile-type germanium dioxide at high pressure. *Phys. Rev. B* **1998**, *58*, No. R2909.

(79) Rosenblum, S. S.; Weber, W. H.; Chamberland, B. L. Raman-scattering observation of the rutile-to-$CaCl_2$ phase transition in RuO_2. *Phys. Rev. B* **1997**, *56*, No. 529.

(80) Hellwig, H.; Goncharov, A. F.; Gregoryanz, E.; Mao, H.-k.; Hemley, R. J. Brillouin and Raman spectroscopy of the ferroelastic rutile-to-$CaCl_2$ transition in SnO_2 at high pressure. *Phys. Rev. B* **2003**, *67*, No. 174110.

(81) Davies, G. F. The Estimation of Elastic Properties from Analogue Compounds. *Geophys. J. Int.* **1976**, *44*, 625−647.

(82) Arashi, H. Raman spectroscopic study of the pressure-induced phase transition in TiO_2. *J. Phys. Chem. Solids* **1992**, *53*, 355−359.